Process parameters variation effect on OFET based low power hydrogen sensor design

YOGESH THAKUR[1], MAMTA KHOSLA[1], BALWANT RAJ[2], SHASHI BALA[3], BALWINDER RAJ[1,*]
[1]*Nanoelectronics Research Lab, Department of Electronics and Communication Engineering NIT Jalandhar, India*
[2]*UIET, Panjab University SSG Regional Centre Hoshiarpur-146001, India*
[3]*Chandigarh Engineering College- CGC Landaran, Mohali, India*

This study takes a unique approach by investigating the influence of various parameters on charge transport processes in Organic Field Effect Transistor (OFET) models. These parameters include field-effect mobility, disorder, trap existence, threshold voltage, and current ON/OFF ratio. The study utilizes two-dimensional finite element-based device models to explore top-contact OFETs with uniform and unequal mobility zones. Several calibrated simulation standards are developed to replicate the morphological disorder in structure, such as considering variable low mobility zones surrounding contacts. The study also examines the effects of varying the channel length from 10 µm to 50 µm on OFF current, ON current, threshold voltage, and current ON/OFF ratio. Notably, the device's Subthreshold slope remains constant for changes in channel length at 68.87 meV/dec. The current ratio decreases with the increase in work function. The sensitivity of both OFF and ON current increases with a change in work function, reaching a maximum value of 705.09 & 0.080 for a 200 meV change at 50 µm channel length.

(Received June 20, 2024; accepted December 2, 2024)

Keywords: OFET, Hydrogen sensor, TCAD simulations, Sub-threshold slope and sensitivity

1. Introduction

OFET applications research has seen a rapid acceleration over the past 30 years. These devices hold great promise in many applications, including low-cost, flexible, lightweight, low fabrication temperature and environmentally friendly semiconductor applications. They are particularly well-suited for active-matrix backplanes in displays, biosensors, gas sensors, and radio frequency identification tags (RFIDs) [1]–[3], despite their lower electron mobility than typical inorganic semiconductors. This potential opens exciting possibilities for the future of semiconductor technology. This potential opens exciting possibilities for the future of semiconductor technology. Inorganic semiconductors, on the other hand, have limited stretching capabilities and so cannot be manufactured on plastic or any other flexible substrate. They also need extra manufacturing stages and a dust-free environment, resulting in a higher fabrication cost. The electrical and chemical characteristics, as well as the electronic structure of these devices, need be properly defined and understood to efficiently construct organic devices that can compete at the same level as inorganic semiconductor devices [4-7]. The commercial benefit of OFETs for next-generation devices is that they may be processed in various methods, such as solution casting, ink-jet printing, spin coating, and so on. Because OFETs have less leakage current, a lower processing temperature, and need fewer fabrication steps than MOSFETs [8], they may be a viable option for bulk-Si transistors in terms of good performance and cheap fabrication costs.

Among other sensor applications, OFET showed potential in biosensors, chemical, pressure, and light sensors [9][10]. Hydrogen, one of the most common gases on earth, is present in water, hydrocarbons, and alcoholic drinks. Natural biomass from plants, animals, and food waste contributes to hydrogen production. [1–3, 6]. Hydrogen gas is frequently referred to as an energy transporter rather than an energy source. Various processes, such as Steam reforming and partial oxidation, can be used to extract hydrogen from fossil fuels [11–13]. Hydrogen gas is colorless and odorless in nature, making it untraceable by human senses. Meanwhile, safety considerations associated with hydrogen uses must be addressed due to its unique features compared to other flammable gases. Such dangerous features include low minimum ignition energy (0.017 mJ), high heat of combustion (143 kJ/g), high diffusivity of hydrogen gas (0.61 cm^2/s in the air) and wide flammable range (4%-75%), which produces a high burning velocity. To detect hydrogen leakage, many high-efficiency H_2 sensors have been created over the last 100 years [5, 14–16]. On the other hand, current H_2 sensors have certain drawbacks, including difficult production processes, poor durability, a need for heating, and an inability to cover a vast area, such as wrapping around hydrogen pipes. As a result, there is still a constant need for hydrogen sensors to satisfy various specifications in several industrial applications.

2. Validation of OFET structure

An OFET is made up of many functional layers. Evaporated small-molecule, solution-cast polymers produce an organic semiconducting layer, a charge transport layer through which electric current flows. For simulation, pentacene is used as an organic semiconducting layer with a thickness of 25 nm and is deposited on the gate dielectric, as shown in Fig. 1. Pentacene is a common organic semiconductor with a HUMO-LUMO bandgap energy of 2.25 eV. The thickness of the gate dielectric is taken as 5.3 nm, which is of 3.6 nm aluminium oxide layer and 1.7 nm SAM layer of n-tetradecyl phosphonic acid offering a capacitance density of 600 nF/cm^2 [17]. To define source/drain (S/D) electrodes, metal contacts were placed on the top. The geometry used for this device simulation is BGTC [18].

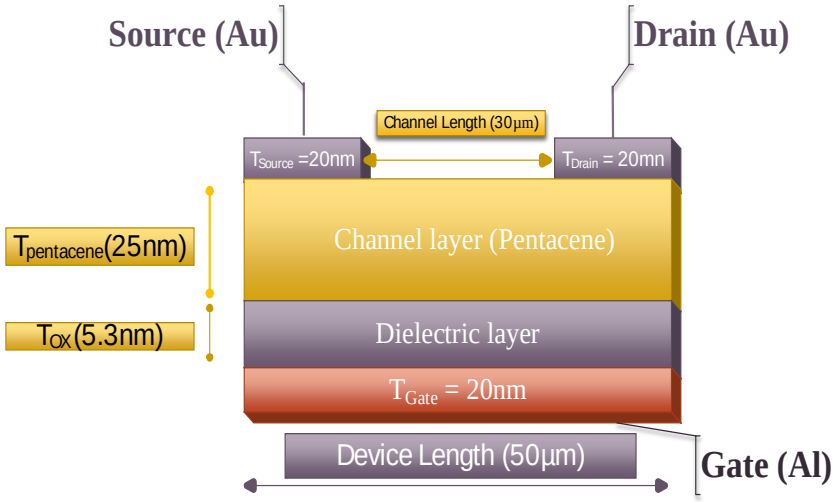

Fig. 1. Schematic Representation of pentacene OFET 2D structure used in simulation (color online)

To calibrate the drain current as in the reported data [17] simulation on Silvaco TCAD [19] is carried out for a long channel length of 30 µm and channel width of 100 µm. In Fig. 1, T_{Source}, T_{Drain}, and T_{Gate} refer to the thickness of the Source, Drain, and Gate electrodes, respectively. The output characteristics are obtained to optimize the paper's results using different models representing FLDMOB (field-dependent mobility) and SRH (Shockley-Read-Hall recombination model), as shown in Fig. 4.

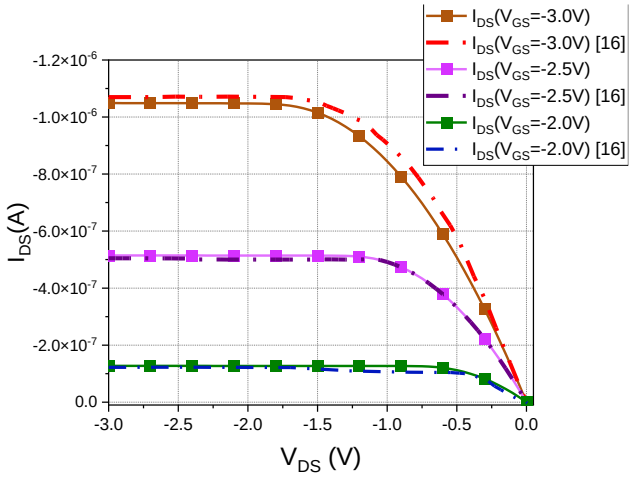

Fig. 2. TCAD simulation results in the following output characteristics matched the results from the paper [16] (color online)

From the results in Fig. 4, it can be observed that the results from reported data [17] are matched with the simulated results. The drain current increases as the gate voltage increases, and a high drain current at gate voltage -3.0 V is obtained.

3. Working principle of H_2 sensor

Pt-based H_2 sensors are widely used as they sense H_2 gas by lattice expansion of electrodes. In this research paper, sensors with different channel lengths having a high dielectric constant (HfO_2) are examined to offer a better response of hydrogen sensors. When exposed to gas molecules, equation (1) determines how the work function of the metal contact changes. Sensitivity is assessed in relation to I_{off}, I_{on}, drain current (I_{DS}), and ON/OFF current ratio (I_{ON}/I_{OFF}) [20].

$$\Delta\varphi_m = cont - \frac{RT}{4F} lnP \quad (1)$$

Here, $\Delta\varphi_m$ is the work function change.
T is temperature.
F is Faraday's constant.
R is the gas constant.
P is partial pressure of the gas.

Recently, preliminary work reviewed hydrogen gas sensors, where it demonstrated that Pt as gate electrode

can show gas sensing. [15]. Therefore, this work aims to study its dynamic behaviour and working principle in detail. After H_2 absorption in this device, the Pt electrode volume is increased. Due to its distinct detecting system, the H_2 sensor can operate at low H_2 concentrations (as low as 200 ppm) without heating up. It also has rapid response and recovery speeds. Because platinum (Pt) metal is sensitive to hydrogen gas molecules, it is utilized at the gate electrode to design hydrogen gas sensors. The work function of platinum metal ranges from 4.5 eV to 4.7 eV [21].

Variations in metal's work function affect the device's ON-state current (I_{ON}), OFF-state current (I_{OFF}), and threshold voltage (V_{th}). Thus, I_{ON}, I_{OFF}, and V_{th} can be used as sensitivity parameters for sensitivity measurements [22,23].

For the developed sensor, sensitivity formulae [20] for OFET w.r.t OFF-state current and ON-state current are presented equations (2) and (3) [24].

$$S_{I_{OFF}} = \frac{I_{OFF(after\ gas\ absorption)}}{I_{OFF(before\ gas\ absorption)}} \quad (2)$$

$$S_{I_{ON}} = \frac{I_{ON(after\ gas\ absorption)} - I_{ON(before\ gas\ absorption)}}{I_{ON(before\ gas\ absorption)}} \quad (3)$$

Fig. 3 shows the proposed OFET for an H_2 sensor based on pentacene as the active layer material. The work function of Pt considered for an H_2 gas sensor is taken as 4.5 eV, where the work function of Pt metal will change while reacting with H_2 gas molecules.

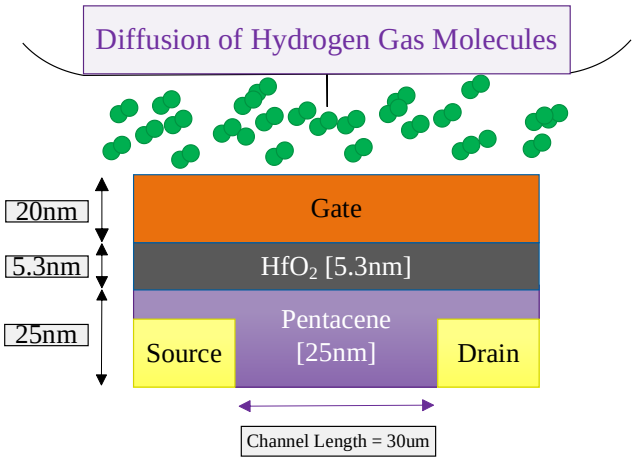

Fig. 3. Proposed p-channel pentacene OFET H_2 gas sensor with exposed hydrogen gas on Pt- Gate electrode in Top Gate Top Contact Geometry (TGTC) of OFET [25] (color online)

The device parameters used to depict the device study are shown in Table 1. The parameters used are similar to the matched simulated data as only the geometry of the device. The device has been inverted from the Bottom Gate Top Contact (BGTC) to TGBC. The reason for doing so is as platinum, the proposed TGTC shape of the OFET will be in direct contact with the gas, allowing for the most significant amount of sensing surface since more gas can fall on the gate electrode while also increasing sensitivity. For the working principle of this OFET device, when sufficient voltage or the provided low-voltage supply is maintained for its working, it shows that the device is supposed to be in an ON state. When hydrogen gas falls on the gate electrode of OFET, where platinum material is used, hydrogen gas interacts with the lattice of platinum atoms and from H_2 gas, they divide into hydrogen atoms and reside inside the platinum electrode. In this case, gas parameters such as gas concentration, gas pressure, and temperature play a huge role. Due to this reaction of hydrogen gas at the gate electrode, a change in the work function of the Pt material is observed. This change in work function will directly influence the drain current of the device, which is why hydrogen gas sensing is observed in the device. Now, for the hydrogen gas field effect transistor that have been simulated, observation found are the transfer and output characteristics of the device.

Table 1. OFET parameters used in the 2D simulation

S. No	Parameter	Values	Units
1	Channel Length (L_g)	30	µm
2	Thickness of Organic Layer ($T_{pentacene}$)	25	nm
3	Dielectric Thickness (T_{ox})	5.3	nm
4	Dielectric material	HfO_2 (22)	
4	Energy Bandgap (E_g)	2.25	eV
5	Electron affinity (E_a)	2.49	eV
6	P-type channel doping (n_i)	2e17	cm^{-3}
7	Work function of gate (φ_{Pt})	4.5	eV
8	Work function of S/D (φ_{Au})	5.0	eV
9	Electron mobility (μ_n)	7e-4	cm^2/V-s
10	Hole Mobility (μ_p)	0.54	cm^2/V-s
11	Poole Frenkel factor	7.758e-8	$eV(V/cm)^{1/2}$
12	Zero-Field activation energy (ΔE_a)	1.792e-7	eV

A pentacene as an active layer is used with a doping of p-type, 30 µm channel length and 25 nm thickness. Source and drain electrodes were made of gold with a work function of 5.0 eV. The primary purpose of this structure is to get maximum gas on the gate electrode so that sensing can be improved. Table 1 depicts the parameters used for this structure more accurately.

To obtain transfer characteristics, -3.0 V is considered as the operating voltage for both gate-source (V_{GS}) and drain-source (V_{DS}), respectively [26].

4. Results and discussion

From the proposed p-channel OFET in Fig. 1, the device's transfer characteristics are extracted by varying V_{DS} from 0 to -4.5 V and keeping V_{GS} constant at -3.0 V for channel lengths varying from 10 to 50 µm. Tables 2 to 6 show the results obtained and the sensitivity regarding ON and OFF current calculated from derived on and off current at change in work function from 0 to 200 meV.

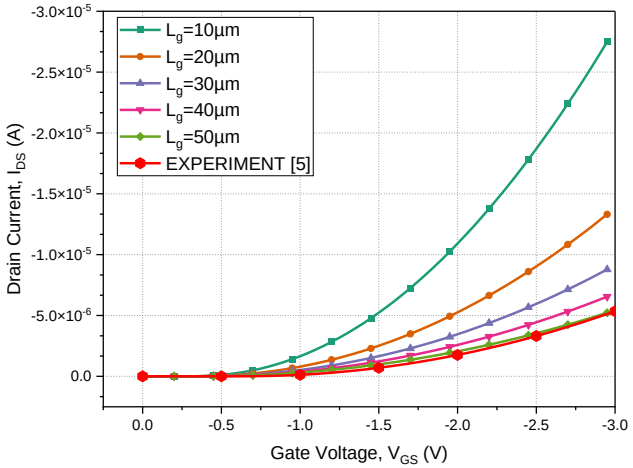

Fig. 4. Transfer Characteristics (I_{DS} - V_{GS}) of OFET with varying channel length and compared with the published literature [5] (color online)

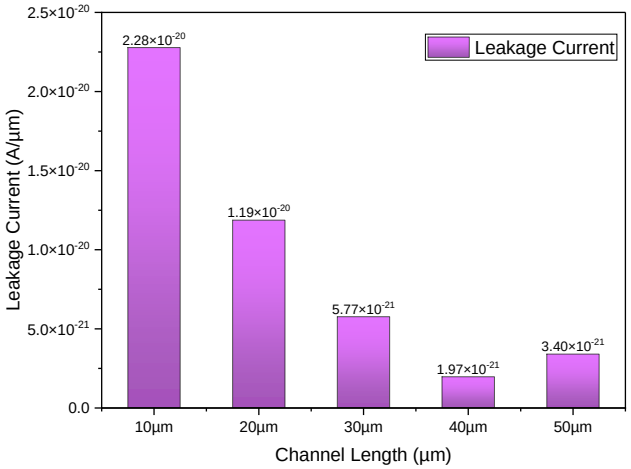

Fig. 5. The leakage current of the device at different channel lengths (color online)

Figs. 4 and 5 show the transfer and leakage currents of the devices with varying channel length values from 10 to 50 µm. Fig. 4 shows the comparison and an increase in the drain current value for a decrease in the device's channel length. This is because the distance between the source and drain decreases with the channel length, and it takes less time for charge carriers to move from source to drain under the influence of a horizontal electric field. In Fig. 5, an increase in leakage current is observed for decreasing channel length, showcasing an increase in electric field, which causes the charge carriers to exert more force to get leaked.

Table 2. Transfer characteristics obtained for OFET of Channel length of 10 µm

$\Delta\varphi_m$	V_{th} (V)	SS (V)	I_{OFF} (A)	I_{ON}(A)	I_{ON}/I_{OFF}	$S_{I_{OFF}}$	$S_{I_{ON}}$
No gas	-0.48	0.0688	-2.46e-13	-6.42e-5	2.60e8	0	--
50	-0.43	0.0688	-1.21e-12	-6.55e-5	5.37e7	4.91	0.02024
100	-0.38	0.0688	-6.17e-12	-6.67e-5	1.08e7	25.08	0.03894
150	-0.33	0.0688	-3.21e-11	-6.80e-5	2.11e6	130.48	0.05919
200	-0.28	0.0695	-1.71e-10	-6.92e-5	4.04e5	695.12	0.07788

Table 3. Transfer characteristics obtained for OFET of Channel length 20 µm

$\Delta\varphi_m$	V_{th} (V)	SS (V)	I_{OFF} (A)	I_{ON} (A)	I_{ON}/I_{OFF}	$S_{I_{OFF}}$	$S_{I_{ON}}$
No gas	-0.56	0.0687	-1.16e-13	-3.16e-5	2.71e8	--	--
50	-0.51	0.0687	-5.78e-13	-3.22e-5	5.57e7	4.98	0.01898
100	-0.46	0.0687	-2.93e-12	-3.28e-5	1.12e7	25.25	0.03797
150	-0.41	0.0687	-1.53e-11	-3.35e-5	2.18e6	131.89	0.06012
200	-0.36	0.0694	-8.17e-11	-3.41e-5	4.17e5	704.31	0.07911

Table 4. Transfer characteristics obtained for OFET of Channel length 30 µm

$\Delta\varphi_m$	V_{th} (V)	SS (V)	I_{OFF} (A)	I_{ON} (A)	I_{ON}/I_{OFF}	$S_{I_{OFF}}$	$S_{I_{ON}}$
No gas	-0.62	0.0687	-7.63e-14	-2.10e-5	2.75e8	--	--
50	-0.57	0.0687	-3.79e-13	-2.14e-5	5.64e7	4.96	0.01904
100	-0.52	0.0687	-1.92e-12	-2.18e-5	1.13e7	25.16	0.03809
150	-0.47	0.0687	-1.00e-11	-2.22e-5	2.21e6	131.06	0.05714
200	-0.42	0.0694	-5.36e-11	-2.26e-5	4.22e5	702.49	0.07619

Table 5. Transfer characteristics obtained for OFET of Channel length 40 µm

$\Delta\varphi_m$	V_{th} (V)	SS (V)	I_{OFF} (A)	I_{ON}(A)	I_{ON}/I_{OFF}	$S_{I_{OFF}}$	$S_{I_{ON}}$
No gas	-0.66	0.0687	-5.67e-14	-1.57e-5	2.77e8	--	--
50	-0.61	0.0687	-2.82e-13	-1.60e-5	5.68e7	4.97	0.01910
100	-0.56	0.0687	-1.43e-12	-1.63e-5	1.14e7	25.22	0.03821
150	-0.51	0.0687	-7.59e-12	-1.66e-5	2.22e6	133.86	0.05732
200	-0.46	0.0693	-3.99e-11	-1.69e-5	4.25e5	703.70	0.07643

Table 6. Transfer characteristics obtained for OFET of Channel length 50 µm

$\Delta\varphi_m$	V_{th} (V)	SS (V)	I_{off} (A)	I_{ON}(A)	I_{ON}/I_{OFF}	$S_{I_{OFF}}$	$S_{I_{ON}}$
No gas	-0.71	0.0687	-4.51e-14	-1.25e-5	2.78e8	--	--
50	-0.66	0.0687	-2.24e-13	-1.28e-5	5.71e7	4.96	0.02400
100	-0.61	0.0687	-1.14e-12	-1.30e-5	1.14e7	25.27	0.04000
150	-0.56	0.0687	-5.95e-12	-1.33e-5	2.23e6	131.92	0.06400
200	-0.51	0.0693	-3.18e-11	-1.35e-5	4.26e5	705.09	0.08000

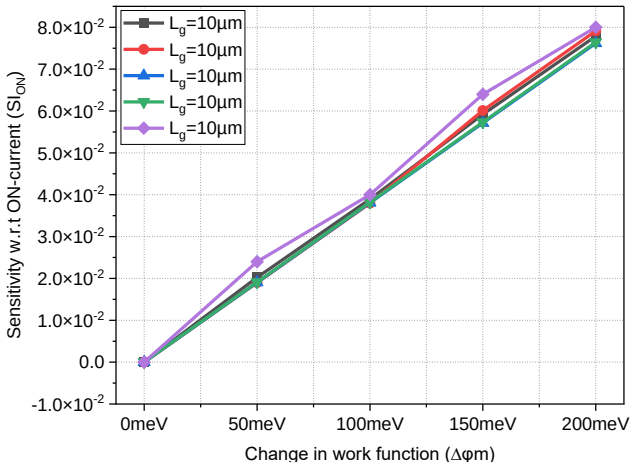

Fig. 6. Sensitivity w.r.t on current for H_2 gas sensor (color online)

Fig. 6 shows the effects of varying channel length on performance parameters, threshold voltage and ON current sensitivity. The sensitivity of an H_2 gas sensor increases with channel length. Sensitivity is determined for various channel lengths (10 µm, 20 µm, 30 µm, 40 µm, and 50 µm), with L_g=10 µm having the maximum sensitivity. The surface-to-volume ratio and gate controllability increase with increasing channel length (L_g), improving the H_2 gas sensor's sensitivity.

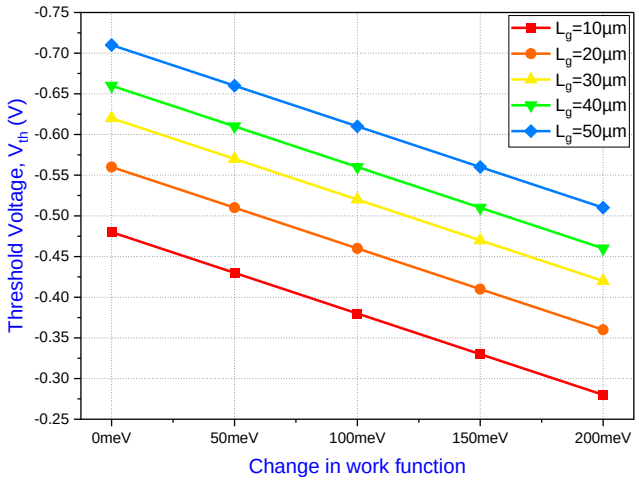

Fig. 7. Change in threshold voltage w.r.t to change in work function for various channel lengths of the device (color online)

Threshold voltage also rises because longer channels require higher gate voltage to accumulate carriers and form an inversion layer, which in turn causes the depletion barrier width to widen. Higher ON state current and threshold voltage are the outcomes, which raise the I_{ON}/I_{OFF} ratio [24] As shown in Fig. 7, shorter channels draw more leakage current, raising the subthreshold swing. SS has an almost ideal value for channel lengths of 10 µm or more (68.78 mV/dec). However, beyond this range, surface potential becomes less sensitive to gate voltage, raising SS.

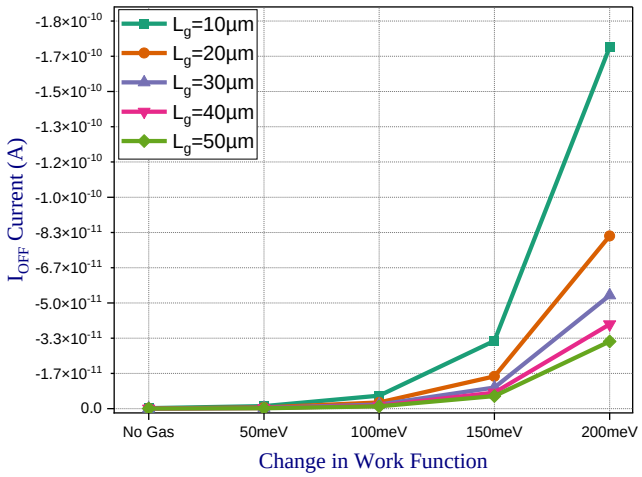

Fig. 8. Variation of OFF current w.r.t change in work function ratio of OFET for varying channel length (color online)

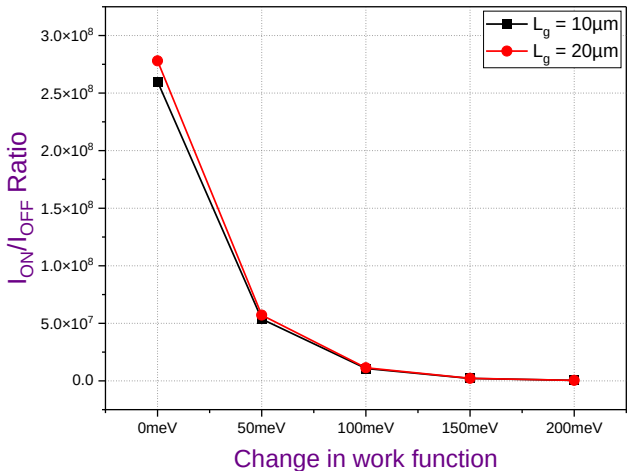

Fig. 9. Variation of Current ON- OFF w.r.t change in work function ratio of OFET for 10 and 50 µm channel length (color online)

Fig. 8 shows the OFF-current value of devices with various channel lengths of the devices. As for the high current ON-OFF ratio, a less OFF current is required for the devices, and its changes depict the observation of sensitivity. So, a better OFF current value is found for 50 µm channel length. Fig. 9 shows variation in the current on-off ratio for 10 & 50 µm channel lengths, where a higher ON/OFF ratio for 50 µm channel length is observed as the number of charge carriers in the channel increases and an increase in OFF current is also observed for the devices with increasing channel length. As the work function of gate metal increases, it generates many charge carriers in the inverted channel [20]. This leads to a decrease in ions, which reduces the I_{ON}/I_{OFF} ratio. OFET works as a p-channel, and the generation of charge carriers inhibits the flow of p-channel semiconductors [20-22].

In conclusion, we can state that OFET performs better in sensitivity for channel lengths 50 µm. However, the threshold voltage of an OFET with a 10 µm channel length was lower. Due to the lower threshold voltage, devices with lower threshold voltages can be used to obtain results at lower gate voltages. A little variation in subthreshold voltage is seen for all the devices with different channel lengths.

5. Conclusion

The design of top gate contact geometry for OFET is proposed, and the performance of this proposed device is analyzed and observed for varying channel lengths. Sensors with higher channel lengths showed higher sensitivity when compared with devices with different channel lengths. Since hydrogen has no colour and no smell, it is highly combustible and difficult to detect, making hydrogen gas sensors vital for safety. They are crucial in averting leaks and mishaps in the transportation, energy, and industrial sectors that utilize hydrogen. In addition, they aid in safety regulation compliance and promote the development of renewable energy technology. To achieve broader usage, sensor technology advancements will concentrate on improving sensitivity, robustness, and integration with intelligent monitoring systems. This device can be further enhanced by using high-k dielectric and other organic materials with higher mobility for optimized results and higher sensitivity.

Conflict of Interest

The authors declare no conflicts of interest.

Author contributions

All authors worked and contributed in the research paper.

Availability of data and material

The article contains the data needed to get the results.

Funding statement: Not applicable

References

[1] S. G. Surya, H. N. Raval, R. Ahmad, P. Sonar, K. N. Salama, V. R. Rao, TrAC Trends in Analytical Chemistry **111**, 27 (2019).
[2] B. Li, P. T. Lai, W. M. Tang, Int. J. Hydrogen Energy **46**, 16232 (2021).
[3] J. Yu, X. Yu, L. Zhang, H. Zeng, Sens. Actuators B Chem. **173**, 133 (2012).
[4] Y. Thakur, B. Raj, S. S. Gill, Optoelectron. Adv. Mat. **17**, 335 (2023).
[5] B. Li, P. T. Lai, W. M. Tang, IEEE Electron Device Letters **38**, 1132 (2017).
[6] P. Kumar, B. Raj, Silicon **14**, 6031 (2021).
[7] P. Kumar, S. K. Sharma, B. Raj, Silicon **3**, 4067 (2021).
[8] P. Kumar, S. S. Gill, Journal of Nanoelectronics and Optoelectronics **13**, 1705 (2018).
[9] Y. Thakur, B. Raj, B. Raj, ECS Journal of Solid State Science and Technology **13**(4), 047005 (2024).
[10] A. Verma, S. Gupta, V. N. Mishra, R. Prakash, IEEE Trans Electron Devices **70**, 2453 (2023).
[11] C. Schwandt, D. J. Fray, Hydrogen Sensing in Molten Aluminium Using a Commercial Electrochemical Sensor, vol. **6**, 2000.
[12] R. Chaubey, S. Sahu, O. O. James, S. Maity, Renewable and Sustainable Energy Reviews **23**, 443 (2013).
[13] N. Sazali, Int. J. Hydrogen Energy **45**, 18753 (2020).
[14] M. Nishibori, W. Shin, N. Izu, T. Itoh, I. Matsubara, S. Yasuda, Int. J. Hydrogen Energy **34**, 2834 (2009).
[15] T. Hübert, L. Boon-Brett, G. Black, U. Banach, Sens. Actuators B Chem. **157**, 329 (2011).
[16] Y. Luo, C. Zhang, B. Zheng, X. Geng, M. Debliquy, Int. J. Hydrogen Energy **42**, 20386 (2017).
[17] A. D. D. Dwivedi, S. K. Jain, R. D. Dwivedi, S. Dadhich, Journal of Science: Advanced Materials and Devices **4**, 561 (2019).
[18] T. Kaimakamis, M. Bucher, M. Gioti, D. Tassis, Org. Electron. **119**, 106812 (2023).
[19] Atlas User's Manual Device Simulation Software, 1984.
[20] R. Gautam, M. Saxena, R. S. Gupta, M. Gupta, IEEE Trans. Nanotechnol **12**, 939 (2013).
[21] J. K. Schaeffer, L. R. C. Fonseca, S. B. Samavedam, Y. Liang, P. J. Tobin, B. E. White, Appl. Phys. Lett. **85**, 1826 (2004).
[22] S. Kim, G. Singh, K. Lee, Adv. Mater. Technol. **7**, 2200180 (2022).
[23] H. Yamazaki, Y. Hayashi, K. Masunishi, D. Ono, T. Ikehashi, Electronics and Communications in Japan **102**, 70 (2019).
[24] N. K. Singh, A. Raman, S. Singh, N. Kumar, Superlattices Microstruct. **111**, 518 (2017).
[25] Y. Thakur, B. Raj, B. Raj, ECS Journal of Solid State Science and Technology **13**, 047005 (2024).
[26] B. Li, P. T. Lai, W. M. Tang, IEEE Trans. Electron Devices **67**, 1776 (2020).

*Corresponding author: rajb@nitj.ac.in